

# Changes in Winter Temperature Extremes from Future Arctic Sea-Ice Loss and Ocean Warming

Y. T. Eunice Lo<sup>1</sup>, Daniel M Mitchell<sup>1</sup>, Peter A. G. Watson<sup>2</sup>, and James A Screen<sup>3</sup>

<sup>1</sup>University of Bristol

<sup>2</sup>School of Geographical Sciences, University of Bristol

<sup>3</sup>University of Exeter

December 16, 2022

## Abstract

Observed rapid Arctic warming and sea-ice loss are likely to continue in the future, unless and after greenhouse gas emissions are reduced to net-zero. Here, we examine the possible effects of future sea-ice loss at 2°C global warming above pre-industrial levels on winter temperature extremes across the Northern Hemisphere, using coordinated experiments from the Polar Amplification Model Intercomparison Project. 1-in-20-year cold extremes are simulated to become less severe at high- and mid-latitudes in response to Arctic sea-ice loss. 1-in-20-year winter warm extremes become warmer at northern high latitudes due to sea-ice loss, but warm by less than cold extremes. We compare the response to sea-ice loss to that from global SST change also at 2°C global warming. SST change causes less severe cold extremes and more severe warm extremes globally. Except northern high latitudes, the response to SST change is of larger magnitude than that to Arctic sea-ice loss.

## Hosted file

952090\_0\_art\_file\_10532592\_rm64b6.docx available at <https://authorea.com/users/518290/articles/613423-changes-in-winter-temperature-extremes-from-future-arctic-sea-ice-loss-and-ocean-warming>

## Hosted file

952090\_0\_supp\_10532555\_rm62p7.docx available at <https://authorea.com/users/518290/articles/613423-changes-in-winter-temperature-extremes-from-future-arctic-sea-ice-loss-and-ocean-warming>



## 18 **Abstract**

19 Observed rapid Arctic warming and sea-ice loss are likely to continue in the future, unless and  
20 after greenhouse gas emissions are reduced to net-zero. Here, we examine the possible effects of  
21 future sea-ice loss at 2°C global warming above pre-industrial levels on winter temperature  
22 extremes across the Northern Hemisphere, using coordinated experiments from the Polar  
23 Amplification Model Intercomparison Project. 1-in-20-year cold extremes are simulated to  
24 become less severe at high- and mid-latitudes in response to Arctic sea-ice loss. 1-in-20-year  
25 winter warm extremes become warmer at northern high latitudes due to sea-ice loss, but warm by  
26 less than cold extremes. We compare the response to sea-ice loss to that from global SST change  
27 also at 2°C global warming. SST change causes less severe cold extremes and more severe warm  
28 extremes globally. Except northern high latitudes, the response to SST change is of larger  
29 magnitude than that to Arctic sea-ice loss.

30

## 31 **Plain Language Summary**

32 The Arctic and neighbouring regions have rapidly warmed in recent decades and the sea ice has  
33 reduced. These changes will likely continue in future, unless greenhouse gas emissions from  
34 human activities are reduced to net-zero. Ongoing sea-ice loss can affect weather and climate  
35 across the Northern Hemisphere. We use climate models to study how extremely cold and hot  
36 temperatures in winter may change because of Arctic sea-ice loss. In a future world that is, on  
37 average, 2°C warmer than pre-industrial times, cold extremes will become less severe at high-  
38 and mid-latitudes because of Arctic sea-ice loss. Winter hot extremes also get warmer, but over  
39 fewer regions and not by as much as cold extremes. In the real world, changes in sea ice happen  
40 alongside changes in ocean temperatures. So, we also looked at the effect of ocean temperature  
41 changes in a 2°C warmer world on winter temperature extremes. Ocean warming will lead to  
42 warmer cold and hot extremes in the Northern Hemisphere. The effect from ocean warming is  
43 larger than that from Arctic sea-ice loss, meaning that even in the few places where sea-ice loss  
44 might cause cooling, it will be overwhelmed by warming due to the ocean temperature changes.

45

46

47

## 48 **1 Introduction**

49 Polar amplification, the phenomenon where near-surface air temperatures near the poles warm  
50 more than the global average in response to external radiative forcing, is a prominent feature of  
51 anthropogenic climate change. Since the late 20<sup>th</sup> century, the Arctic has warmed 3 to 4 times  
52 faster than the global mean (Rantanen et al., 2022), and September Arctic sea-ice extent has  
53 decreased by half (Francis & Wu, 2020). Arctic amplification is driven by local temperature,  
54 surface albedo and cloud feedbacks, and changes in the poleward transport of energy in the  
55 atmosphere and ocean (Goosse et al., 2018; Previdi et al., 2021). It is strongest in boreal winter.  
56 Climate models have been shown to be able to reproduce the observed temperature and mean sea

57 ice trends in the Arctic, albeit with demonstrated discrepancies in other variables (Notz & SIMIP  
58 Community, 2020; Previdi et al., 2021).

59 Previous modelling studies have projected a decrease in the likelihood and duration of cold  
60 extremes at the high latitudes and over central and eastern North America, but not over central  
61 Asia, due to future Arctic sea-ice loss (Screen et al., 2015a, 2015b). Another study has projected  
62 no change in the frequency or duration of cold weather outbreaks but a decrease in their severity  
63 in the US, Europe and East Asia (Ayarzagüena & Screen, 2016).

64 By contrast, winter warm extremes in relation to Arctic changes are much less studied.  
65 Increasingly for the Arctic region, however, mild winter conditions are becoming a concern  
66 because short-lived warm spells in winter are associated with rain on snow events. These events  
67 have wide-ranging impacts on vegetation, soil organisms, Arctic species, and human livelihoods,  
68 and they are projected to become more frequent in future (Serreze et al., 2021). Novel work is  
69 needed to investigate changes in winter warm extremes due to future Arctic sea-ice loss.

70 Furthermore, there is uncertainty about the influence of Arctic amplification on atmospheric  
71 circulation and mid-latitude severe weather (Cohen et al., 2020; Overland et al., 2021). For  
72 example, coupled atmosphere-ocean models suggest that Arctic sea-ice loss intensifies the  
73 wintertime Siberian High, but the temperature response is not robustly simulated (Labe et al.,  
74 2020; Screen et al., 2018; Screen & Blackport, 2019). Uncertainty comes from the different  
75 climate models, different forcings and methodologies, and in some cases, relatively small  
76 ensembles used (Cohen et al., 2020; Overland et al., 2016; Smith et al., 2019). This provides a  
77 strong rationale for using coordinated experiments in a large multi-model ensemble.

78 The Polar Amplification Model Intercomparison Project (PAMIP) provides a set of coordinated  
79 experiments designed to understand the causes as well as the consequences of polar  
80 amplification (Smith et al., 2019). It is a contribution to the Coupled Model Intercomparison  
81 Project Phase 6 (CMIP6) (Eyring et al., 2016). By running standardized experiments in different  
82 climate models and generating large ensembles from each model, PAMIP helps to provide a  
83 better estimate of the forced response and to quantify model uncertainty (Screen et al., 2018).  
84 PAMIP simulations have been used to study, for instance, the effects of Arctic sea-ice loss  
85 and/or warming on the North Pacific jet stream (Ronalds et al., 2020), poleward heat transport  
86 (Audette et al., 2021), the wintertime Siberian High (Labe et al., 2020), and mid-latitude westerly  
87 winds (Smith et al., 2022).

88 Here, we utilize the atmosphere-only PAMIP experiments for the first time to assess the  
89 respective responses of boreal winter cold and warm extremes to future Arctic sea-ice loss and  
90 sea surface temperature (SST) change associated with 2°C global mean warming above pre-  
91 industrial levels. We focus on land regions in the Northern Hemisphere, where extreme  
92 temperatures have direct impacts on their communities. Using daily temperature output from ten  
93 PAMIP models, each of which having up to 200 ensemble members, we examine the changes in  
94 1-in-20-year cold and warm events. Expanding on previous studies, we study both cold and hot  
95 extremes and also examine the respective responses to sea-ice loss and SST change.

96 Consideration of the response to SST change is important, as the local cooling in response to sea-  
97 ice loss proposed in earlier studies may be overwhelmed by warming due to global SST change.

98

## 99 **2 Data and Methods**

### 100 **2.1 PAMIP experiments**

101 We compare model-simulated temperatures between three PAMIP atmosphere-only time slice  
102 experiments. First, we use an experiment forced by present-day (i.e., 1979-2008 climatological)  
103 SSTs and sea-ice concentration (Smith et al., 2019), denoted as 'pd' hereafter. Second, we use an  
104 experiment forced by present-day SSTs but future Arctic sea-ice concentration representative of  
105 2°C global average warming above pre-industrial levels. This experiment is denoted as  
106 'futArcSIC'. Third, we make use of an experiment in which climate models are forced by future  
107 SSTs representative of 2°C global warming but sea-ice concentration at the present-day level.  
108 This experiment is referred to as 'futSST'. We note that 2°C global average warming above pre-  
109 industrial levels is equivalent to 15.7°C in absolute global mean temperature, and that sea ice  
110 thickness changes are not included in these experiments (Smith et al., 2019). All of these  
111 experiments are one-year time slices with radiative forcing from the year 2000. As such,  
112 comparing futArcSIC with pd provides an estimate of extreme temperature changes due to future  
113 Arctic sea-ice concentration loss, whereas comparing futSST with pd provides an estimate of  
114 changes due to future SST change.

115 These experiments are run by climate models with a minimum of ~100 winters to generate large  
116 ensembles that are suitable for studying climate extremes (Smith et al., 2019). We make use of  
117 daily minimum (tasmin) and maximum (tasmax) near-surface air temperature outputs from ten  
118 climate models, as listed in supplementary Table S1. Specifically, we focus on the respective  
119 changes in minimum tasmin and maximum tasmax in boreal winter (December-January-  
120 February, or DJF) due to future Arctic sea-ice loss and SST change. All included models have  
121 daily tasmin and tasmax outputs for pd and futArcSIC. A subset of six models also have outputs  
122 for futSST. More than half of the models have at least 200 ensemble members. We use a  
123 maximum of 200 members from each model to compute the differences in 1-in-20-year winter  
124 minimum and maximum temperatures at each model grid point due to Arctic sea-ice loss and  
125 SST change. A 1-in-20-year event has a 5% chance of occurring in any given year, and we use it  
126 to represent extremes. A maximum of 200 members is a large enough sample size for this return  
127 period, but more members could have been used from some models (Table 1) (Thompson et al.,  
128 2017). By focusing on DJF minimum and maximum temperatures, we avoid averaging out the  
129 extremes in seasonal means (Francis, 2021). We conduct an additional return period analysis at  
130 the regional scale (Sections 2.2 and 2.3).

131 The included models have different atmospheric horizontal resolutions, ranging from 0.83° x  
132 0.56° in HadGEM3-GC31-MM (Andrews et al., 2020) to ~2.8° in CanESM5 (Swart et al., 2019).  
133 For all grid cells in the Northern Hemisphere, we calculate the difference in 1-in-20-year  
134 minimum and maximum temperatures between the PAMIP experiments in individual models, as  
135 well as the multi-model mean difference (giving each model equal weight). When considering  
136 the individual models, we compute the temperature difference in the models' native grids. When

137 considering the multi-model mean, we regrid (through nearest-neighbour regriding) all model  
138 results to CanESM5's grid because it is the coarsest among the studied models, before computing  
139 the multi-model mean difference.

140

## 141 **2.2 Regions**

142 We perform analyses in 14 selected regions in the northern mid to high latitudes. These regions  
143 are selected from a pre-defined set of regions that are  $\sim 2 \text{ Mm}^2$  in size and designed for  
144 examining climate extremes and their impacts (Stone, 2019). The regions are shown in Figure  
145 S1.

146

## 147 **2.3 Return period analyses**

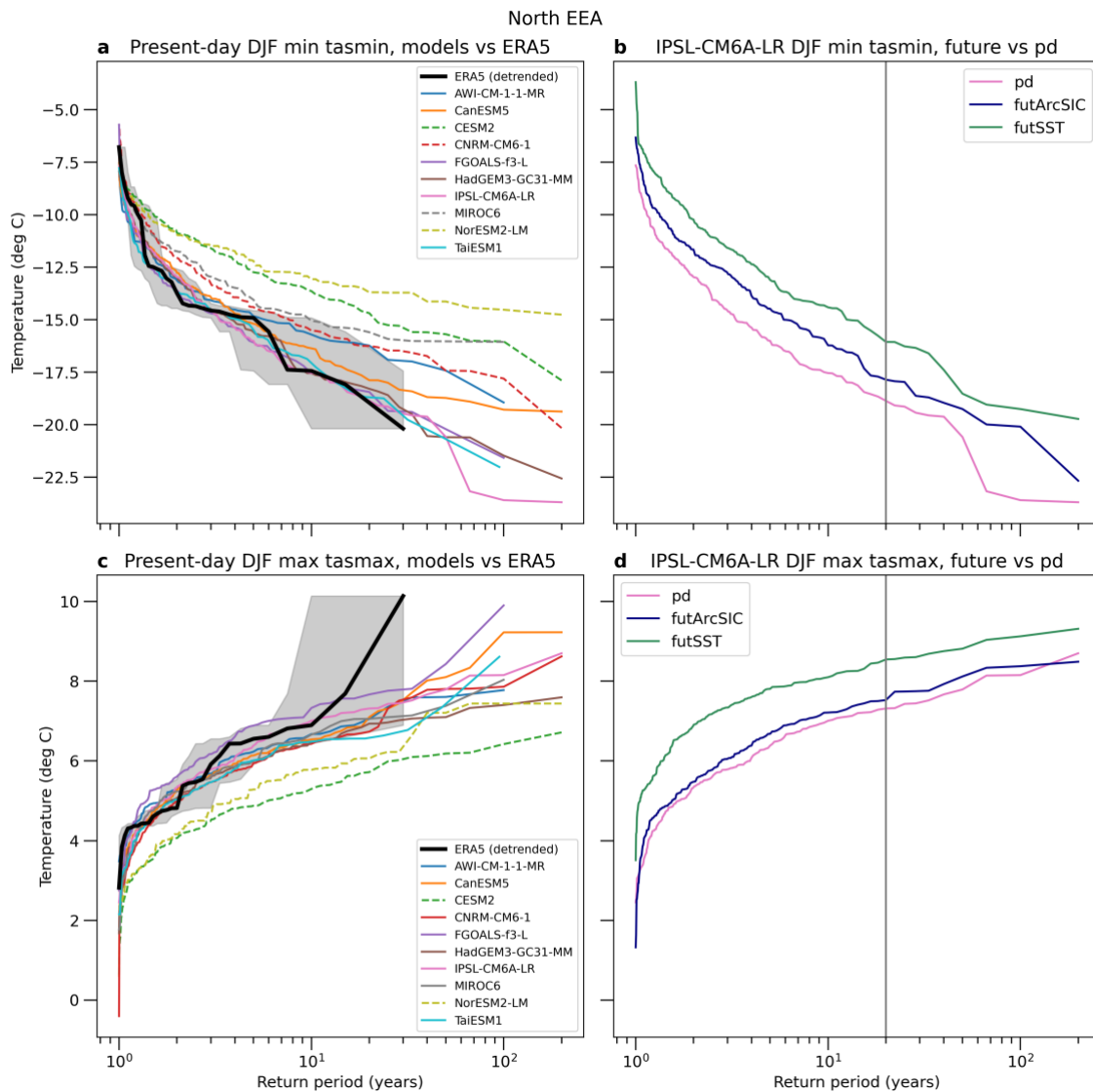
148 We compute return periods by sorting each temperature series of DJF minimum tasmin (and  
149 maximum tasmax) in ascending (descending) order and dividing the length of the series by the  
150 ranks of the temperature values within the sorted series. We find the difference in 1-in-20-year  
151 temperature between experiments at each model grid point. We test whether the two samples of  
152 temperatures (i.e., not just the 1-in-20-year values) from different experiments are significantly  
153 different using a Kolmogorov-Smirnov (KS) test (Daniel, 1990).

154 For the regional analysis, we produce and compare return period curves from the pd simulations  
155 and the ERA5 reanalysis (Hersbach et al., 2020). We find the regional mean DJF minimum  
156 tasmin and maximum tasmax by area-weighted averaging values across native grid cells whose  
157 grid point values are within the boundary of each region. Since the present-day conditions in pd  
158 are based on 1979-2008 climatology, we extract ERA5 data from the same time period for  
159 comparison. This comparison is not completely like-for-like because inter-annual variability  
160 exists in ERA5 but not in pd, which has constant boundary forcing. To remove the climate  
161 change signal from the regional ERA5 time series and approximately isolate internal variability,  
162 we fit a linear trend to the corresponding DJF mean tasmin (and tasmax) time series and remove  
163 this trend from the 1979-2008 DJF minimum tasmin (maximum tasmax) time series. This  
164 ensures that the trends in the winter season, not just in the extremes, are removed. We then add  
165 the regional 1995-2005 average DJF minimum tasmin (maximum tasmax) value in ERA5 to the  
166 detrended data, to obtain absolute temperatures for comparison with model output. We choose  
167 the 1995-2005 decade because it is centred on year 2000, the year from which radiative forcing  
168 is used in the PAMIP time slice experiments.

169 The modelled pd data do not need detrending because they come from large ensembles of time  
170 slice simulations and use a constant radiative forcing. To bias-correct data from each model, we  
171 remove from each ensemble member the bias between ensemble-mean regional-mean DJF  
172 minimum tasmin (maximum tasmax) and the corresponding 1979-2008 mean regional-mean

173 ERA5 value. We then find the return period curves based on bias-corrected pd data and  
 174 detrended ERA5 data.

175 We estimate the uncertainty associated with the ERA5 return period curve by resampling the  
 176 ERA5 distribution 1000 times, though acknowledging that uncertainty sampling in the extremes  
 177 is limited by the observations. The comparison between individual model return period curves  
 178 and the ERA5 90% confidence interval enables us to identify models that simulate present-day  
 179 winter temperature extremes reasonably well in the selected regions. Figures 1a and 1c show this  
 180 comparison for North EEA, for which four and two models (indicated by dotted lines) are  
 181 excluded in model selection for cold and warm extremes, respectively, because their return  
 182 period curves are outside the ERA5 envelope at a majority of return periods.



183

184 **Figure 1.** Return period curves for North EEA. (a) The comparison between present-day bias-  
 185 corrected DJF minimum daily minimum temperature data from individual climate models  
 186 (colored lines) and detrended ERA5 over the period 1979-2008 (thick black line). The grey

187 envelope shows the 90% uncertainty associated with the ERA5 curve found by bootstrapping.  
188 Solid colored lines indicate models that are included because they largely fall within the ERA5  
189 envelope, whereas dashed colored lines indicate excluded models. (b) Example results from the  
190 IPSL-CM6A-LR model only, showing DJF minimum daily minimum temperatures in the pd  
191 (pink line), futArcSIC (navy line) and futSST (green line) experiments. The grey vertical line  
192 indicates the 20-year return period. (c) Same as (a) but for DJF maximum of daily maximum  
193 temperature. (d) Same as (b) but for DJF maximum of daily maximum temperature.

194

195 To assess the effects of future Arctic sea-ice concentration loss and SST change on regional  
196 winter extremes, we find the return period curves using the futArcSIC and futSST ensembles,  
197 respectively. Example return period curves from futArcSIC, futSST and pd simulated by IPSL-  
198 CM6A-LR for the North EEA region are shown Figures 1b and 1d. For each model and region,  
199 we find the temperature difference between futArcSIC and pd, and between futSST and pd, at  
200 the 20-year return period. For analyses involving futArcSIC, we report the temperature  
201 differences from the individual models, as well as the multi-model mean across all 10 models  
202 and the mean across a subset of models that simulate the present day well (according to ERA5).  
203 This subset varies from region to region and between cold and warm extremes (Figure S2). For  
204 analyses involving futSST, we mainly report the multi-model mean temperature difference  
205 across the 6 models for which there is output for this experiment (Table S1) for brevity.

206

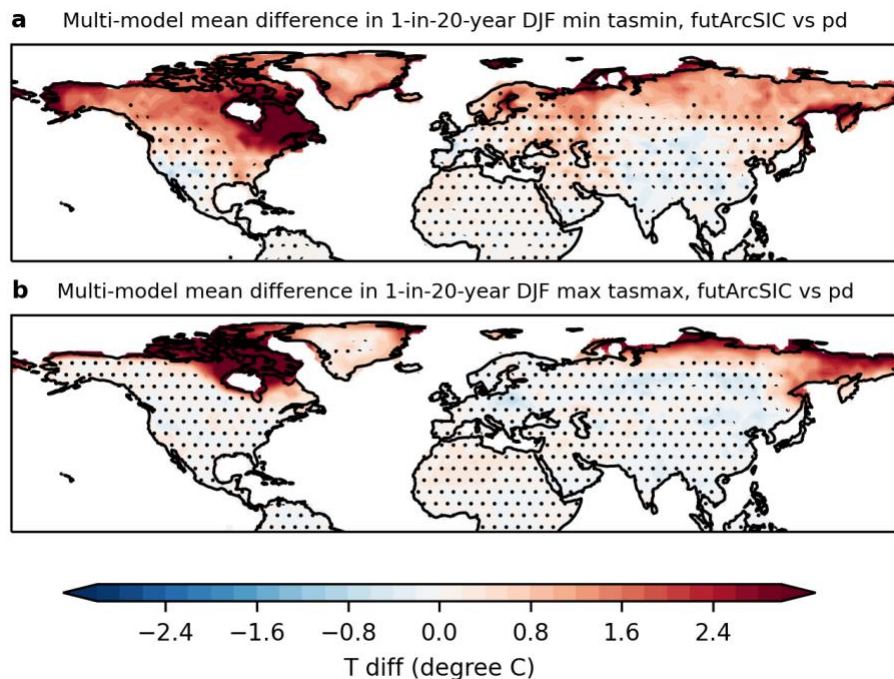
## 207 **3 Results**

### 208 **3.1 Responses to sea-ice loss**

209 Figure 2a shows the multi-model-mean difference in 1-in-20-year winter cold extremes between  
210 futArcSIC and pd in the Northern Hemisphere. The largest warming, of over  $\sim 2.5^{\circ}\text{C}$ , is projected  
211 for northern and eastern Canada near Hudson Bay. The futArcSIC and pd winter minimum  
212 temperature distributions are statistically significantly different at the 5% level, indicating  
213 amplified warming in boreal winter cold extremes due to future Arctic sea-ice loss, as global  
214 average temperature is  $1.4^{\circ}\text{C}$  higher in futArcSIC than in pd (Smith et al., 2019). A statistically  
215 significant warming of  $\sim 2^{\circ}\text{C}$  is also projected for Alaska. These results are generally consistent  
216 across the models (Figure S3), likely due the close proximity to imposed sea ice reductions in  
217 Hudson Bay, Labrador Sea and Bering-Chukchi Seas (Smith et al., 2022).

218 In the multi-model mean,  $\sim 1^{\circ}\text{C}$  warming is simulated in Greenland, across Scandanavia and in  
219 northern Russia. However, there is inconsistency in the sign between the models, with MIROC6  
220 and TaiESM1 simulating some cooling in central Greenland, CanESM5 and CESM2 simulating  
221 cooling over Scandanavia, and four models simulating cooling in different parts of north Russia  
222 (Figure S3). At the mid and low latitudes, cooling responses are seen for the United States, parts  
223 of Europe and central and eastern Asia. In some models, this cooling is up to about  $-1^{\circ}\text{C}$ ,  
224 suggesting intensified winter cold extremes. However, this response is not statistically significant

225 and is less robust in terms of spatial extent and magnitude than the aforementioned higher-  
 226 latitude warming response (Figure S3).



227

228 **Figure 2.** Changes in 1-in-20-year (a) DJF minimum of daily minimum temperature and (b) DJF  
 229 maximum of daily maximum temperature in the Northern Hemisphere due to future Arctic sea-  
 230 ice loss. The panels show the multi-model mean across ten PAMIP models. Stippling indicates  
 231 where the temperature distributions from futArcSIC and pd are not statistically significantly  
 232 different at the 5% level, based on a KS test.

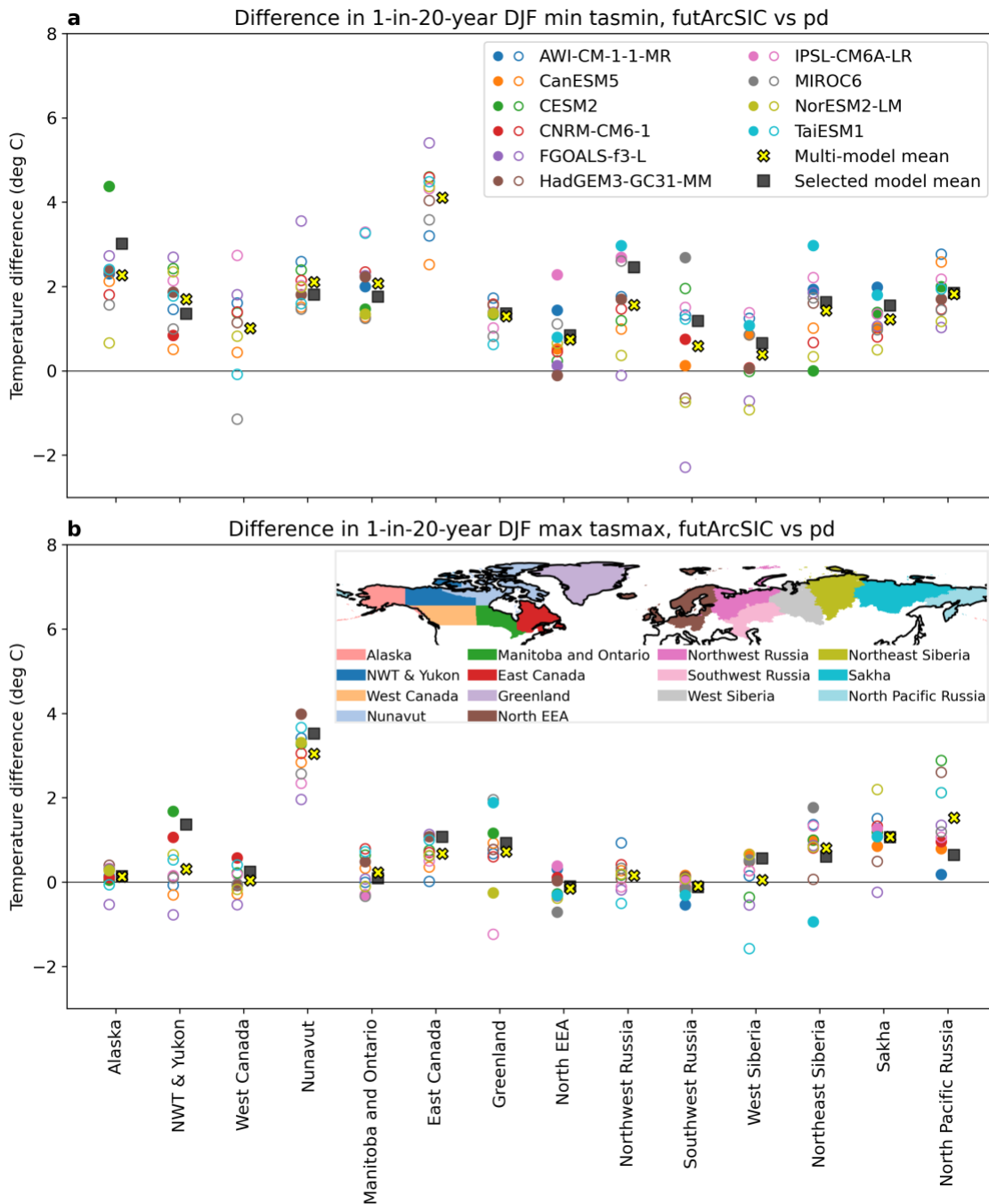
233

234 Figure 2b shows the multi-model-mean difference in 1-in-20-year winter warm extremes  
 235 between futArcSIC and pd. Statistically significant changes are only simulated in the high  
 236 latitudes, with northern Canada showing the strongest warming, of over  $\sim 2.5^{\circ}\text{C}$ , followed by  
 237 northeastern Russia ( $\sim 2^{\circ}\text{C}$ ). These changes are generally consistent across the models (Figure  
 238 S4). The multi-model-mean indicates widespread cooling of up to  $-0.4^{\circ}\text{C}$  that is not statistically  
 239 significant across most parts of North America, Eurasia and central Africa. Individual models  
 240 simulate a stronger cooling response in different parts of the continents, although the responses  
 241 are not statistically significant (Figure S4). A greater warming of cold extremes (Figures 2a and  
 242 S3) compared to warm extremes (Figures 2b and S4) implies reduced temperature variance.

243

244 Next, we examine the regionally averaged differences in 1-in-20-year winter cold and warm  
 245 extremes between futArcSIC and pd in 14 selected regions over the mid-to-high northern  
 246 latitudes, where the largest and most significant temperature responses are simulated. Figure 3  
 247 shows the results from the individual models (circles), as well as the multi-model-mean  
 248 responses across the 10 models (yellow crosses) and the multi-model-mean responses across

249 selected models (i.e., those that simulate regional present-day climates that are consistent with  
 250 the ERA5 reanalysis; black squares).



251

252 **Figure 3.** Temperature differences in (a) DJF minimum daily minimum temperature and (b) DJF  
 253 maximum daily maximum temperature with a 20-year return period between futArcSIC and pd,  
 254 in 14 chosen regions (locations of which are shown in the inset). Each circle represents one  
 255 PAMIP model, with a filled circle indicating consistency between that model's corresponding  
 256 bias-corrected pd return period curve and the equivalent ERA5 return period curve from 1979-

257 2008 for the region, and an empty circle indicating inconsistency with ERA5. Black squares  
258 show the mean across the selected models indicated by the filled circles. Yellow crosses show  
259 the mean across all ten models.

260

261 Like in Figure 2a, the regional analysis for cold extremes (Figure 3a) reveals the largest average  
262 warming response in East Canada, with the models simulating regional-mean warming between  
263 2 and 6°C. In the multi-model mean, all selected regions are projected to experience a warming  
264 of winter cold extremes due to Arctic sea-ice loss, with values ranging from 0.4°C (inter-model  
265 range: -0.9 to 1.4°C) in West Siberia to 4.1°C (range: 2.5 to 5.4°C) in East Canada. The mean  
266 results are similar across the subsets of models (note, no model is consistent with ERA5 in East  
267 and West Canada even after mean bias correction). Despite the general warming response seen in  
268 the multi-model mean, some models simulate intensified winter cold extremes in regions  
269 including West Canada, North EEA, Northwest and Southwest Russia, and West and Northeast  
270 Siberia. However, these cooling responses are not statistically significant (Figure S3) and could  
271 be due to internal variability.

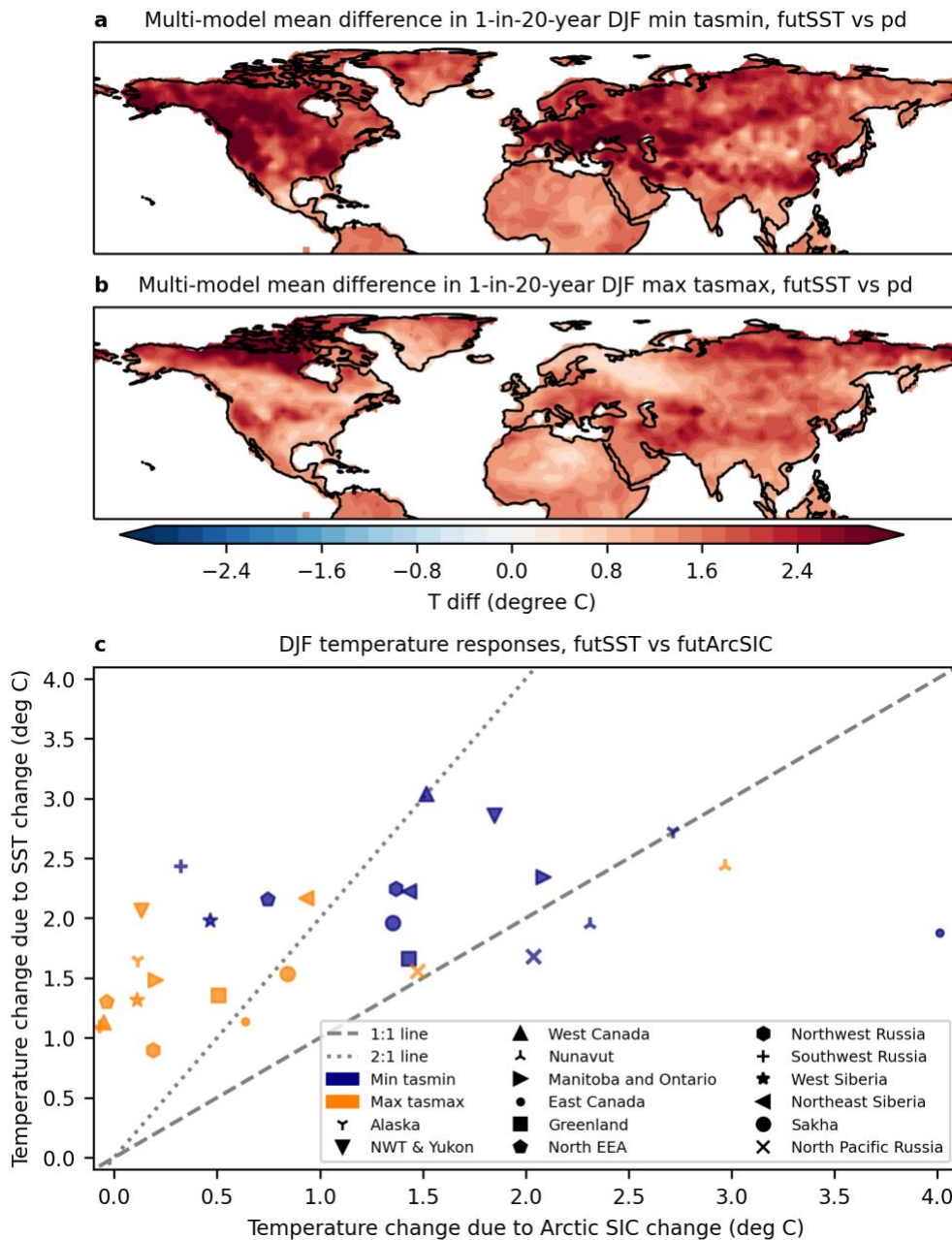
272 The regional results for winter warm extremes are shown in Figure 3b. Nunavut in northern  
273 Canada has the largest multi-model-mean warming response to future Arctic sea-ice loss, with  
274 individual models simulating 2 to 4°C warming. As shown in Figure 2b, North Pacific Russia  
275 has the second largest mean response at 1.5°C (range: 0.2 to 2.9°C). For the rest of the regions,  
276 the multi-model-mean response is within about +/- 1°C, ranging from -0.2°C (range: -0.7 to  
277 0.4°C) in North EEA to 1.1°C (range: -0.2 to 2.2°C) in Sakha. Eleven of the 14 selected regions  
278 (except Nunavut, East Canada and North Pacific Russia) have at least one model simulating a  
279 cooling response, showing a smaller signal-to-noise ratio than cold extremes. Overall, Figure 3  
280 shows that the pd model simulations do not compare very well with reanalysis even after bias  
281 correction, partially because of the idealized nature of the experiments. However, this does not  
282 affect our main results.

283

### 284 **3.2 Responses to SST change**

285 Figure 4a shows that warmer SSTs associated with 2°C global mean warming increase 1-in-20-  
286 year cold temperatures over land in the Northern Hemisphere in the multi-model mean. This  
287 warming is statistically significant at the 5% level. No cooling response is shown in the multi-  
288 model mean at any location. In general, individual models agree on a strong (~3°C) warming  
289 signal in North America, particularly in the western parts (Figure S5). The cold response in  
290 Eurasia to future SST change is more variable, with IPSL-CM6A-LR showing strong warming in

291 the northern parts, whereas FGOALS-f3-L shows cooling in those parts but relatively strong  
 292 warming in east Asia (Figure S5). These differences may be affected by sampling variability.



293

294 **Figure 4.** (a) Multi-model mean changes in 1-in-20-year DJF minimum of daily minimum  
 295 temperature in the Northern Hemisphere due to future SST change. The temperature distributions  
 296 from futSST and pd are statistically significantly different at the 5% level based on a KS test. (b)  
 297 Same as (a) but for DJF maximum of daily maximum temperature. (c) Comparison between the  
 298 multi-model mean temperature changes due to future Arctic sea-ice loss (x-axis) and the  
 299 corresponding changes due to future SST change (y-axis). Navy points indicate changes in 1-in-  
 300 20-year DJF minimum of daily minimum temperature, whereas orange points indicate changes in

301 1-in-20-year DJF maximum of daily maximum temperature. Each point represents the regional  
302 mean in one particular region. The dashed line indicates a 1:1 relationship, whereas the dotted  
303 line indicates a 2:1 relationship.

304

305 Future SST change is also projected to warm winter warm extremes significantly in all Northern  
306 Hemisphere land grid cells in the multi-model mean, as shown in Figure 4b. However, both the  
307 multi-model mean and individual model results (Figure S6) indicate that the warm extreme  
308 response is smaller compared to the cold extreme response in almost all places except northern  
309 Canada. Small inter-model differences are seen in the warm extreme response to SST change,  
310 with CanESM5 simulating cooling in Greenland and northeastern Russia that is not statistically  
311 significant, for example.

312 With previous evidence that responses to sea ice and greenhouse gas forcing are approximately  
313 linearly additive (McCusker et al., 2017), it may be reasonable to deduce the combined mean 1-  
314 in-20-year winter temperature responses to Arctic sea-ice loss and ocean warming from Figures  
315 3 and 4. For cold extremes, even in places where Arctic sea-ice loss is simulated to intensify  
316 them (e.g., in southwestern United States, parts of Europe, central and eastern Asia, though not  
317 statistically significantly; Figure S3), warming due to SST change overwhelms this cooling  
318 effect, resulting in net warming (not shown).

319 Indeed, by comparing the multi-model mean of the 1-in-20-year cold temperature differences  
320 due to Arctic sea-ice change (x-axis) and SST change (y-axis) over the 14 selected regions in  
321 Figure 4c (navy markers), we find that the warming response to future SST change is larger than  
322 or equal to the response to future Arctic sea-ice loss in 11 regions (i.e., except Nunavut, East  
323 Canada and North Pacific Russia). The three exceptions suggest that the response to sea-ice loss  
324 is by far the largest near the regions of sea-ice loss, whereas warming due to SST change is more  
325 spatially homogeneous. The ratio of SST change-induced response to sea ice loss-induced  
326 response ranges from 0.5 in East Canada to 7.5 in Southwest Russia. Since all selected regions  
327 are projected to experience multi-model-mean warming to both sea-ice and SST changes, an  
328 enhanced combined response is expected. For East Canada, this may mean a combined response  
329 of 5.8°C.

330 For warm extremes, warming from SST change also dominates over the small and non-  
331 statistically significant Arctic sea ice-loss induced cooling responses in North America, Eurasia  
332 and Africa, resulting in net warming. Figure 4c shows this clearly, where all but one orange  
333 markers (i.e., except for Nuavut) are above the 1:1 identity line. The ratio of the magnitude of  
334 SST-induced response to the magnitude of sea ice-induced response ranges from 0.8 in Nunavut  
335 to 35 in North EEA (because of a near-zero response to sea ice). In Nunavut (northern Canada),  
336 where winter warm extreme is projected to become statistically significantly warmer due to  
337 Arctic sea-ice loss and SST change separately, the combined effect may mean intensification of

338 warm extremes by 5.4°C, although we emphasize that our results are based on idealized  
339 atmosphere-only experiments.

340

## 341 **5 Discussion and Conclusions**

342 Arctic amplification has been a topic of interest in the literature, not only because it is one of the  
343 strongest anthropogenic climate change signals, but also because of its wide-reaching effects on  
344 the climate system (Labe et al., 2020; Screen et al., 2013). This study is the first to use targeted  
345 and coordinated PAMIP experiments to examine the response of rare (1-in-20-year) winter  
346 temperature extremes to Arctic sea-ice loss and SST change at 2°C global mean warming above  
347 pre-industrial levels. It is also the first to investigate winter warm extremes, and to bias-correct  
348 the PAMIP simulations and apply model selection based on reanalysis data.

349 We have shown a multi-model-mean warming response of winter cold extremes to future Arctic  
350 sea-ice loss across the mid and high latitudes. This is consistent with the projected decrease in  
351 the likelihood and severity of mid- and high-latitude cold extremes in previous studies  
352 (Ayarzagüena & Screen, 2016; Screen et al., 2015b). For 8 of the 14 selected regions (excluding  
353 West Canada, North EEA, Northwest and Southwest Russia, and West and Northeast Siberia),  
354 the sign of change is robust across ten models. Where a local cooling response is simulated in  
355 some models, the location of this cooling is not robust across models, and may be a sign of  
356 internal variability. We cannot rule out a weak cooling response, as suggested by previous  
357 studies (Labe et al., 2020; Zappa et al., 2021), but it appears to be model dependent.

358 The winter cold extreme response to future SST change is more robust, with almost all of the  
359 Northern Hemisphere showing a warming response in all available models. Notably, this  
360 warming response exceeds the sea ice-induced cooling response in southwestern United States,  
361 western Europe, and central and eastern Asia. Overall, our results imply that some of the adverse  
362 impacts of cold extremes on, for instance, human health (Mäkinen, 2007; Vasconcelos et al.,  
363 2013) and transport and power supply (Screen et al., 2015b) are expected to be lessened in the  
364 mid and high latitudes in the future. However, we stress that Arctic warming and sea-ice loss are  
365 already impacting the Arctic communities (Moerlein & Carothers, 2012), whose lifestyles and  
366 livelihoods were adapted to cold weather through generations of lived knowledge.

367 For winter warm extremes, we have shown that statistically significant responses to future Arctic  
368 sea-ice loss are limited to the high latitudes, primarily to northern Canada and northeastern  
369 Russia. Non-significant responses are found for the rest of the hemisphere, and overall the warm  
370 extreme response is weaker than the cold response. This suggests a reduced winter temperature  
371 variance due to Arctic sea-ice loss, which is consistent with the literature (Blackport et al., 2021;  
372 Collow et al., 2019; Screen, 2014). SST-induced warming is larger than the sea ice-induced  
373 changes in most places.

374 Warming of winter warm extremes in the high latitudes due to Arctic sea-ice loss and ocean  
375 warming can increase the chances of rain on snow events. Notable events have already occurred  
376 in Arctic Canada (Rennert et al., 2009) and Russia (Forbes et al., 2016), which led to declines in  
377 ungulate (e.g., reindeer and musk oxen) populations that persisted for years and herders losing

378 food security and transportation (Serreze et al., 2021). Our results suggest that these communities  
379 are at an increased risk of these impacts in a 2°C warmer world, compared to the present day.

380 Sea-ice loss does not happen in isolation, but considering it together with future ocean warming  
381 is not routinely done. Going forward, we recommend researchers place a stronger focus on the  
382 SST component or the net response. Moreover, the combined effect of Arctic sea-ice loss and  
383 SST change on winter temperature extremes has not been studied here. Potential non-linearities  
384 in their effects may mean that a combined future sea-ice and SST experiment in PAMIP is  
385 important. Future work should also quantify the resulting impacts on various aspects of society  
386 through coupled climate and impact modelling.

387 Aside from sea-ice concentration loss and SST change, PAMIP provides a range of experiments  
388 designed to investigate the impacts of sea-ice thickness changes and full ocean dynamics (Smith  
389 et al., 2019), which have not been studied here. Our estimates of the responses to sea-ice loss  
390 may be conservative because both ice thickness changes (Labe et al., 2018) and atmosphere-  
391 ocean coupling (Deser et al., 2015, 2016; Smith et al., 2017) have been suggested to strengthen  
392 the response. It is recommended that researchers fully exploit the PAMIP data to investigate the  
393 effects of these changes.

394

## 395 **Acknowledgments**

396 We thank Tim Woollings for providing feedback to this manuscript. This work was funded by  
397 the NERC grant ArctiCONNECT (grant ID: NE/V005855/1). PAGW was supported by a NERC  
398 Independent Research Fellowship (grant no. NE/S014713/1). The authors have no conflicts of  
399 interests.

400

## 401 **Availability Statement**

402 The PAMIP data used in this study are available at Earth System Grid Federation (ESGF) via  
403 <https://esgf-node.llnl.gov/search/cmip6/>. A user guide for creating an ESGF account and  
404 downloading the data can be found at <https://esgf.github.io/esgf-user-support/>. PAMIP data  
405 information from each modeling center, including their contact information, can be found at  
406 <https://www.cesm.ucar.edu/projects/CMIP6/PAMIP/>. The ERA5 reanalysis data are available  
407 from the Copernicus Climate Data Store  
408 <https://cds.climate.copernicus.eu/cdsapp#!/dataset/reanalysis-era5-single-levels?tab=overview>.

409

## 410 **References**

- 411 Andrews, M. B., Ridley, J. K., Wood, R. A., Andrews, T., Blockley, E. W., Booth, B., et al.  
412 (2020). Historical Simulations With HadGEM3-GC3.1 for CMIP6. *Journal of Advances in*  
413 *Modeling Earth Systems*, 12(6), 1–34. <https://doi.org/10.1029/2019MS001995>
- 414 Audette, A., Fajber, R. A., Kushner, P. J., Wu, Y., Peings, Y., Magnusdottir, G., et al. (2021).  
415 Opposite Responses of the Dry and Moist Eddy Heat Transport Into the Arctic in the

- 416 PAMIP Experiments. *Geophysical Research Letters*, 48(9), 1–10.  
417 <https://doi.org/10.1029/2020GL089990>
- 418 Ayarzagüena, B., & Screen, J. A. (2016). Future Arctic sea ice loss reduces severity of cold air  
419 outbreaks in midlatitudes. *Geophysical Research Letters*, 43(6), 2801–2809.  
420 <https://doi.org/10.1002/2016GL068092>
- 421 Blackport, R., Fyfe, J. C., & Screen, J. A. (2021). Decreasing subseasonal temperature variability  
422 in the northern extratropics attributed to human influence. *Nature Geoscience*, 14(10), 719–  
423 723. <https://doi.org/10.1038/s41561-021-00826-w>
- 424 Cohen, J., Zhang, X., Francis, J., Jung, T., Kwok, R., Overland, J., et al. (2020). Divergent  
425 consensus on Arctic amplification influence on midlatitude severe winter weather. *Nature*  
426 *Climate Change*, 10(1), 20–29. <https://doi.org/10.1038/s41558-019-0662-y>
- 427 Collow, T. W., Wang, W., & Kumar, A. (2019). Reduction in northern midlatitude 2-m  
428 temperature variability due to Arctic sea ice loss. *Journal of Climate*, 32(16), 5021–5035.  
429 <https://doi.org/10.1175/JCLI-D-18-0692.1>
- 430 Daniel, W. W. (1990). *Applied Nonparametric Statistics* (2nd ed.). PWS-KENT Pub.
- 431 Deser, C., Tomas, R. A., & Sun, L. (2015). The role of ocean-atmosphere coupling in the zonal-  
432 mean atmospheric response to Arctic sea ice loss. *Journal of Climate*, 28(6), 2168–2186.  
433 <https://doi.org/10.1175/JCLI-D-14-00325.1>
- 434 Deser, C., Sun, L., Tomas, R. A., & Screen, J. (2016). Does ocean coupling matter for the  
435 northern extratropical response to projected Arctic sea ice loss? *Geophysical Research*  
436 *Letters*, 43(5), 2149–2157. <https://doi.org/10.1002/2016GL067792>
- 437 Eyring, V., Bony, S., Meehl, G. A., Senior, C. A., Stevens, B., Stouffer, R. J., & Taylor, K. E.  
438 (2016). Overview of the Coupled Model Intercomparison Project Phase 6 (CMIP6)  
439 experimental design and organization. *Geoscientific Model Development*, 9(5), 1937–1958.  
440 <https://doi.org/10.5194/gmd-9-1937-2016>
- 441 Forbes, B. C., Kumpula, T., Meschtyb, N., Laptander, R., MacIas-Fauria, M., Zetterberg, P., et  
442 al. (2016). Sea ice, rain-on-snow and tundra reindeer nomadism in Arctic Russia. *Biology*  
443 *Letters*, 12(11), 4–8. <https://doi.org/10.1098/rsbl.2016.0466>
- 444 Francis, J. A. (2021). RE: Article misidentifies study as “landmark.” Retrieved November 29,  
445 2022, from <https://www.science.org/doi/10.1126/comment.763356/full/>
- 446 Francis, J. A., & Wu, B. (2020). Why has no new record-minimum Arctic sea-ice extent  
447 occurred since September 2012? *Environmental Research Letters*, 15(11).  
448 <https://doi.org/10.1088/1748-9326/abc047>
- 449 Goosse, H., Kay, J. E., Armour, K. C., Bodas-Salcedo, A., Chepfer, H., Docquier, D., et al.  
450 (2018). Quantifying climate feedbacks in polar regions. *Nature Communications*, 9(1).  
451 <https://doi.org/10.1038/s41467-018-04173-0>

- 452 Hersbach, H., Bell, B., Berrisford, P., Hirahara, S., Horányi, A., Muñoz-Sabater, J., et al. (2020).  
 453 The ERA5 global reanalysis. *Quarterly Journal of the Royal Meteorological Society*,  
 454 (March), 1–51. <https://doi.org/10.1002/qj.3803>
- 455 Labe, Z., Peings, Y., & Magnusdottir, G. (2018). Contributions of Ice Thickness to the  
 456 Atmospheric Response From Projected Arctic Sea Ice Loss. *Geophysical Research Letters*,  
 457 45(11), 5635–5642. <https://doi.org/10.1029/2018GL078158>
- 458 Labe, Z., Peings, Y., & Magnusdottir, G. (2020). Warm Arctic, Cold Siberia Pattern: Role of  
 459 Full Arctic Amplification Versus Sea Ice Loss Alone. *Geophysical Research Letters*,  
 460 47(17), 1–11. <https://doi.org/10.1029/2020GL088583>
- 461 Mäkinen, T. M. (2007). Human cold exposure, adaptation, and performance in high latitude  
 462 environments. *American Journal of Human Biology*, 19(2), 155–164.  
 463 <https://doi.org/10.1002/ajhb.20627>
- 464 McCusker, K. E., Kushner, P. J., Fyfe, J. C., Sigmond, M., Kharin, V. V., & Bitz, C. M. (2017).  
 465 Remarkable separability of circulation response to Arctic sea ice loss and greenhouse gas  
 466 forcing. *Geophysical Research Letters*, 44(15), 7955–7964.  
 467 <https://doi.org/10.1002/2017GL074327>
- 468 Moerlein, K. J., & Carothers, C. (2012). Total Environment of Change: Impacts of Climate  
 469 Change and Social Transitions on Subsistence Fisheries in Northwest Alaska. *Ecology and*  
 470 *Society*, 17(1). <https://doi.org/10.5751/es-04543-170110>
- 471 Notz, D., & SIMIP Community. (2020). Arctic Sea Ice in CMIP6. *Geophysical Research Letters*,  
 472 47(10), 1–11. <https://doi.org/10.1029/2019GL086749>
- 473 Overland, J. E., Dethloff, K., Francis, J. A., Hall, R. J., Hanna, E., Kim, S. J., et al. (2016).  
 474 Nonlinear response of mid-latitude weather to the changing Arctic. *Nature Climate Change*,  
 475 6(11), 992–999. <https://doi.org/10.1038/nclimate3121>
- 476 Overland, J. E., Ballinger, T. J., Cohen, J., Francis, J. A., Hanna, E., Jaiser, R., et al. (2021). How  
 477 do intermittency and simultaneous processes obfuscate the Arctic influence on midlatitude  
 478 winter extreme weather events? *Environmental Research Letters*, 16(4).  
 479 <https://doi.org/10.1088/1748-9326/abdb5d>
- 480 Previdi, M., Smith, K. L., & Polvani, L. M. (2021). Arctic amplification of climate change: a  
 481 review of underlying mechanisms. *Environmental Research Letters*, 16(9), 093003.  
 482 <https://doi.org/10.1088/1748-9326/ac1c29>
- 483 Rantanen, M., Karpechko, A. Y., Lipponen, A., Nordling, K., Hyvärinen, O., Ruosteenoja, K., et  
 484 al. (2022). The Arctic has warmed nearly four times faster than the globe since 1979.  
 485 *Communications Earth & Environment*, 3(168), 1–10. [https://doi.org/10.1038/s43247-022-](https://doi.org/10.1038/s43247-022-00498-3)  
 486 [00498-3](https://doi.org/10.1038/s43247-022-00498-3)
- 487 Rennert, K. J., Roe, G., Putkonen, J., & Bitz, C. M. (2009). Soil thermal and ecological impacts  
 488 of rain on snow events in the circumpolar arctic. *Journal of Climate*, 22(9), 2302–2315.

- 489 <https://doi.org/10.1175/2008JCLI2117.1>
- 490 Ronalds, B., Barnes, E. A., Eade, R., Peings, Y., & Sigmond, M. (2020). North Pacific zonal  
491 wind response to sea ice loss in the Polar Amplification Model Intercomparison Project and  
492 its downstream implications. *Climate Dynamics*, 55(7–8), 1779–1792.  
493 <https://doi.org/10.1007/s00382-020-05352-w>
- 494 Screen, J. A. (2014). Arctic amplification decreases temperature variance in northern mid- to  
495 high-latitudes. *Nature Climate Change*, 4(7), 577–582.  
496 <https://doi.org/10.1038/nclimate2268>
- 497 Screen, J. A., & Blackport, R. (2019). How Robust is the Atmospheric Response to Projected  
498 Arctic Sea Ice Loss Across Climate Models? *Geophysical Research Letters*, 46(20), 11406–  
499 11415. <https://doi.org/10.1029/2019GL084936>
- 500 Screen, J. A., Simmonds, I., Deser, C., & Tomas, R. (2013). The atmospheric response to three  
501 decades of observed arctic sea ice loss. *Journal of Climate*, 26(4), 1230–1248.  
502 <https://doi.org/10.1175/JCLI-D-12-00063.1>
- 503 Screen, J. A., Deser, C., & Sun, L. (2015a). Projected changes in regional climate extremes  
504 arising from Arctic sea ice loss. *Environmental Research Letters*, 10(8).  
505 <https://doi.org/10.1088/1748-9326/10/8/084006>
- 506 Screen, J. A., Deser, C., & Sun, L. (2015b). Reduced risk of North American cold extremes due  
507 to continued arctic sea ice loss. *Bulletin of the American Meteorological Society*, 96(9),  
508 1489–1503. <https://doi.org/10.1175/BAMS-D-14-00185.1>
- 509 Screen, J. A., Deser, C., Smith, D. M., Zhang, X., Blackport, R., Kushner, P. J., et al. (2018).  
510 Consistency and discrepancy in the atmospheric response to Arctic sea-ice loss across  
511 climate models. *Nature Geoscience*, 11(3), 155–163. <https://doi.org/10.1038/s41561-018-0059-y>
- 513 Serreze, M. C., Gustafson, J., Barrett, A. P., Druckenmiller, M. L., Fox, S., Voveris, J., et al.  
514 (2021). Arctic rain on snow events: Bridging observations to understand environmental and  
515 livelihood impacts. *Environmental Research Letters*, 16(10). <https://doi.org/10.1088/1748-9326/ac269b>
- 517 Smith, D. M., Dunstone, N. J., Scaife, A. A., Fiedler, E. K., Copsey, D., & Hardiman, S. C.  
518 (2017). Atmospheric response to Arctic and Antarctic sea ice: The importance of ocean-  
519 atmosphere coupling and the background state. *Journal of Climate*, 30(12), 4547–4565.  
520 <https://doi.org/10.1175/JCLI-D-16-0564.1>
- 521 Smith, D. M., Screen, J. A., Deser, C., Cohen, J., Fyfe, J. C., García-Serrano, J., et al. (2019).  
522 The Polar Amplification Model Intercomparison Project (PAMIP) contribution to CMIP6:  
523 investigating the causes and consequences of polar amplification. *Geoscientific Model*  
524 *Development Discussions*, 12, 1139–1164. <https://doi.org/10.5194/gmd-12-1139-2019>
- 525 Smith, D. M., Eade, R., Andrews, M. B., Ayres, H., Clark, A., Chripko, S., et al. (2022). Robust

- 526 but weak winter atmospheric circulation response to future Arctic sea ice loss. *Nature*  
527 *Communications*, 13(1), 1–15. <https://doi.org/10.1038/s41467-022-28283-y>
- 528 Stone, D. A. (2019). A hierarchical collection of political/economic regions for analysis of  
529 climate extremes. *Climatic Change*, 155(4), 639–656. <https://doi.org/10.1007/s10584-019-02479-6>
- 531 Swart, N. C., Cole, J. N. S., Kharin, V. V., Lazare, M., Scinocca, J. F., Gillett, N. P., et al.  
532 (2019). The Canadian Earth System Model version 5 (CanESM5.0.3). *Geoscientific Model*  
533 *Development*, 12(11), 4823–4873. <https://doi.org/10.5194/gmd-12-4823-2019>
- 534 Thompson, V., Dunstone, N. J., Scaife, A. A., Smith, D. M., Slingo, J. M., Brown, S., & Belcher,  
535 S. E. (2017). High risk of unprecedented UK rainfall in the current climate. *Nature*  
536 *Communications*, 8(1), 1–6. <https://doi.org/10.1038/s41467-017-00275-3>
- 537 Vasconcelos, J., Freire, E., Almendra, R., Silva, G. L., & Santana, P. (2013). The impact of  
538 winter cold weather on acute myocardial infarctions in Portugal. *Environmental Pollution*,  
539 183, 14–18. <https://doi.org/10.1016/j.envpol.2013.01.037>
- 540 Zappa, G., Ceppi, P., & Shepherd, T. G. (2021). Eurasian cooling in response to Arctic sea-ice  
541 loss is not proved by maximum covariance analysis. *Nature Climate Change*, 11(2), 106–  
542 108. <https://doi.org/10.1038/s41558-020-00982-8>

#### 543 **References from Supplementary Materials**

- 544 Andrews, M. B., Ridley, J. K., Wood, R. A., Andrews, T., Blockley, E. W., Booth, B., et al.  
545 (2020). Historical Simulations With HadGEM3-GC3.1 for CMIP6. *Journal of Advances in*  
546 *Modeling Earth Systems*, 12(6), 1–34. <https://doi.org/10.1029/2019MS001995>
- 547 Boucher, O., Servonnat, J., Albright, A. L., Aumont, O., Balkanski, Y., Bastrikov, V., et al.  
548 (2020). Presentation and Evaluation of the IPSL-CM6A-LR Climate Model. *Journal of*  
549 *Advances in Modeling Earth Systems*, 12(7), 1–52. <https://doi.org/10.1029/2019MS002010>
- 550 Danabasoglu, G., Lamarque, J. F., Bacmeister, J., Bailey, D. A., DuVivier, A. K., Edwards, J., et  
551 al. (2020). The Community Earth System Model Version 2 (CESM2). *Journal of Advances*  
552 *in Modeling Earth Systems*, 12(2), 1–35. <https://doi.org/10.1029/2019MS001916>
- 553 He, B., Bao, Q., Wang, X., Zhou, L., Wu, X., Liu, Y., et al. (2019). CAS FGOALS-f3-L Model  
554 Datasets for CMIP6 Historical Atmospheric Model Intercomparison Project Simulation.  
555 *Advances in Atmospheric Sciences*, 36(8), 771–778. <https://doi.org/10.1007/s00376-019-9027-8>
- 557 Seland, Ø., Bentsen, M., Seland Graff, L., Olivié, D., Toniazzo, T., Gjermundsen, A., et al.  
558 (2020). The Norwegian Earth System Model, NorESM2 – Evaluation of the CMIP6 DECK  
559 and historical simulations. *Geoscientific Model Development Discussions*, (February), 1–68.  
560 <https://doi.org/10.5194/gmd-2019-378>
- 561 Semmler, T., Danilov, S., Gierz, P., Goessling, H. F., Hegewald, J., Hinrichs, C., et al. (2020).

- 562 Simulations for CMIP6 With the AWI Climate Model AWI-CM-1-1. *Journal of Advances*  
563 *in Modeling Earth Systems*, 12(9), 1–34. <https://doi.org/10.1029/2019MS002009>
- 564 Swart, N. C., Cole, J. N. S., Kharin, V. V., Lazare, M., Scinocca, J. F., Gillett, N. P., et al.  
565 (2019). The Canadian Earth System Model version 5 (CanESM5.0.3). *Geoscientific Model*  
566 *Development*, 12(11), 4823–4873. <https://doi.org/10.5194/gmd-12-4823-2019>
- 567 Tatebe, H., Ogura, T., Nitta, T., Komuro, Y., Ogochi, K., Takemura, T., et al. (2019).  
568 Description and basic evaluation of simulated mean state, internal variability, and climate  
569 sensitivity in MIROC6. *Geoscientific Model Development*, 12(7), 2727–2765.  
570 <https://doi.org/10.5194/gmd-12-2727-2019>
- 571 Voltaire, A., Saint-Martin, D., Sénési, S., Decharme, B., Alias, A., Chevallier, M., et al. (2019).  
572 Evaluation of CMIP6 DECK Experiments With CNRM-CM6-1. *Journal of Advances in*  
573 *Modeling Earth Systems*. <https://doi.org/10.1029/2019MS001683>
- 574 Wang, Y. C., Hsu, H. H., Chen, C. A., Tseng, W. L., Hsu, P. C., Lin, C. W., et al. (2021).  
575 Performance of the Taiwan Earth System Model in Simulating Climate Variability  
576 Compared With Observations and CMIP6 Model Simulations. *Journal of Advances in*  
577 *Modeling Earth Systems*, 13(7), 1–28. <https://doi.org/10.1029/2020MS002353>